Published in final edited form as:
Acta Biomater. 2015 February ; 13: 159–167. doi:10.1016/j.actbio.2014.11.030.

High strength, surface porous polyether-ether-ketone for load-bearing orthopaedic implants

Nathan T. Evans[†,*,a], **F. Brennan Torstrick**[†,b,c], **Christopher S.D. Lee**[d], **Kenneth M. Dupont**[e], **David L. Safranski**[e], **W. Allen Chang**[d], **Annie E. Macedo**[f], **Angela Lin**[b,c], **Jennifer M. Boothby**[f], **Daniel C. Whittingslow**[f], **Robert A. Carson**[b], **Robert E. Guldberg**[b,c], and **Ken Gall**[a,b,c]

F. Brennan Torstrick: brennan@gatech.edu; Christopher S.D. Lee: chris.lee@verteraspine.com; Kenneth M. Dupont: kenneth.dupont@medshape.com; David L. Safranski: david.safranski@medshape.com; W. Allen Chang: allen.chang@verteraspine.com; Annie E. Macedo: amacedo@gatech.edu; Angela Lin: angela.lin@me.gatech.edu; Jennifer M. Boothby: jboothby3@gatech.edu; Daniel C. Whittingslow: dwhittingslow@gatech.edu; Robert A. Carson: robert.carson@gatech.edu; Robert E. Guldberg: robert.guldberg@ibb.gatech.edu; Ken Gall: ken.gall@mse.gatech.edu

[a]School of Materials Science and Engineering, 771 Ferst Drive, J. Erskine Love Building, Georgia Institute of Technology, Atlanta, GA 30332

[b]George W. Woodruff School of Mechanical Engineering, 801 Ferst Drive, Georgia Institute of Technology, Atlanta, GA 30332

[c]Parker H. Petit Institute for Bioengineering and Bioscience, 315 Ferst Drive, Georgia Institute of Technology, Atlanta, GA 30332

[d]Vertera, Inc., 311 Ferst Drive NW Suite L1328, Atlanta, GA 30332

[e]MedShape, Inc., 1575 Northside Drive, NW, Suite 440, Atlanta, GA 30318

[f]Wallace H. Coulter Department of Biomedical Engineering, 313 Ferst Drive, Georgia Institute of Technology and Emory University, Atlanta, GA 30332

Abstract

Despite its widespread clinical use in load-bearing orthopaedic implants, polyether-ether-ketone (PEEK) is often associated with poor osseointegration. In this study, a surface porous PEEK material (PEEK-SP) was created using a melt extrusion technique. The porous layer thickness was 399.6±63.3 μm and possessed a mean pore size of 279.9±31.6 μm, strut spacing of 186.8±55.5 μm, porosity of 67.3±3.1%, and interconnectivity of 99.9±0.1%. Monotonic tensile tests showed that PEEK-SP preserved 73.9% of the strength (71.06±2.17 MPa) and 73.4% of the elastic modulus (2.45±0.31 GPa) of as-received, injection molded PEEK. PEEK-SP further demonstrated

[*]Corresponding Author, **Contact Information:**, Evans: nevans3@gatech.edu, 404-660-4418.
[†]These authors contributed equally to this work.

Disclosures

K.M.D and D.L.S are employees of MedShape, Inc. and C.S.D.L., K.M.D, D.L.S, K.G. own stock/stock options in MedShape, Inc. C.S.D.L. and W.A.C. are employees of Vertera, Inc. and N.T.E., F.B.T. C.S.D.L., W.A.C., K.M.D., D.L.S., D.C.W., R.E.G., and K.G. own stock/stock options in Vertera, Inc.

a fatigue strength of 60.0 MPa at one million cycles, preserving 73.4% of the fatigue resistance of injection molded PEEK. Interfacial shear testing showed the pore layer shear strength to be 23.96±2.26 MPa. An osseointegration model in the rat revealed substantial bone formation within the pore layer at 6 and 12 weeks via μCT and histological evaluation. Ingrown bone was more closely apposed to the pore wall and fibrous tissue growth was reduced in PEEK-SP when compared to non-porous PEEK controls. These results indicate that PEEK-SP could provide improved osseointegration while maintaining the structural integrity necessary for load-bearing orthopaedic applications.

Keywords

polyetheretherketone (PEEK); fatigue; surface porous; orthopaedic implant

1. Introduction

The ultimate goal of most medical implants is to restore impaired biological function and achieve functional integration with the body. Several porous polymers and other tissue engineered scaffolds have made advances in this regard for many soft tissue applications where mechanical loading is minimal [1]. However, similar solutions in high load-bearing orthopaedic environments remain elusive due to performance tradeoffs in clinically adopted biomaterials. Metallic implants provide high strength but are associated with medical imaging artifacts and unwanted bone resorption due to their high modulus and corresponding stress shielding [2]. Current porous polymer scaffolds can facilitate bony ingrowth but lack the strength necessary for high load-bearing environments experienced in clinical soft tissue reconstructions, spinal fusions, and arthrodesis applications [3, 4]. Bioresorbable polymers and composites facilitate osseointegration and implant resorption, but are clinically limited to soft tissue reconstructions and have cited incidences of prolonged inflammation, migration, incomplete degradation, and implant breakage [5].

As a relatively new implant material, polyether-ether-ketone (PEEK) has gained widespread acceptance as a high-strength polymer used primarily in spinal fusions and soft tissue reconstructions, with favorable imaging compatibility and stiffness that closely matches bone [6, 7]. However, PEEK suffers a key property tradeoff in poor osseointegration. Its aromatic backbone and semi-crystalline nature provide high strength and biocompatibility, yet its hydrophobic and chemically inert surface limits local bone attachment [8, 9].

Basic research approaches to enhance PEEK osseointegration have focused both on surface modification and bulk porosity. Surface modifications such as plasma or chemical etching [10–12], addition of bioactive coatings [13, 14], and PEEK composites have performed well *in vitro* and *in vivo* [15], yet their clinical success may be limited due to their potential instability and delamination in physiological or surgical environments [16, 17]. Introducing bulk porosity throughout PEEK implants via powder sintering (or compression molding) aims to increase implant fixation by encouraging the migration and proliferation of various cell types to enhance vascular and bone tissue ingrowth [3, 18]. Indeed, porous PEEK implants have exhibited increased osseointegration [15]; however, they also suffered up to

86% reduction in strength due to the high overall fraction of porosity and the relatively weak local bonds created during powder sintering [3, 19, 20].

Limiting porosity to PEEK's surface could promote osseointegration and maintain bulk mechanical properties [19]. Furthermore, a surface porosity approach is supported by the finding that a completely porous structure may not be required for functional integration [19, 21]. A porous surface layer could retain implant strength, provide an adequate conduit for bone ingrowth, and avoid tissue necrosis common at the center of large fully porous implants in cases of limited vascular and nutrient supply [22, 23].

Here we investigate a novel method to create a functionally graded PEEK material with a balance between surface porosity for osseointegration and a solid core for mechanical load-bearing. Porous and solid regions are seamlessly connected, resulting in outstanding mechanical properties compared to powder sintering or coatings [3]. Samples are created using a patent-pending technique in which PEEK is extruded through sodium chloride crystals to create a surface porosity. The resulting structure and properties of the surface porous PEEK are discussed as well as preliminary *in vivo* results to provide initial insight into its potential to osseointegrate.

2. Materials and Methods

2.1 Sample Preparation

Surface porous PEEK (PEEK-SP) samples were created by extruding medical grade PEEK (Zeniva® 500, Solvay Advanced Polymers, T_m=340°C) through the lattice spacing of sodium chloride crystals (Sigma Aldrich) under heat and pressure. After cooling, embedded sodium chloride crystals were leached in water leaving behind a porous surface layer. To control for pore size, sodium chloride was sieved into a range of 200–312 μm using #50 and #70 U.S. mesh sieves. Injection molded PEEK samples (PEEK) were used as smooth controls. Powder sintered bulk porous samples (PEEK-BP) were created using a compression molding technique [6]. Briefly, sodium chloride and PEEK powder (KetaSpire® KT-820FP, Solvay Advanced Polymers) were thoroughly mixed at a ratio to achieve equivalent pore size and porosity as PEEK-SP. Powder mixtures were sintered under 260 MPa compression for 60 minutes at 363°C within a 10 mm diameter cylindrical mold (Heated Manual Press, Model 4386, Carver, Inc.). Sodium chloride was leached in water and sodium chloride removal was confirmed via microcomputed tomography (μCT). Poly(methyl methacrylate) (PMMA, McMaster-Carr), a polymer commonly used as bone cement in orthopaedic surgery, was used as a control for monotonic tension and tensile fatigue studies.

All tensile specimens were ASTM D638 Type I dog-bone samples. Shear samples were cut from PEEK bars to have a cross-sectional shear area of 16×16 mm for PEEK and PEEK-SP or 10 mm diameter for PEEK-BP. *In vivo* implants were 5 mm diameter cylinders machined to a length of 8 mm from PEEK bars. One face was made surface porous while the other face was machined smooth as a control. A hole was bored through the center to replace the native medullary cavity.

2.2 Pore Layer Characterization

PEEK-SP samples were cut to size and the porous layers were scanned using μCT (μCT 50; Scanco Medical) at 10 μm voxel resolution with the scanner set at a voltage of 55 kVp and a current of 200 μA (n=15). Surface porous layers were manually contoured tightly to the pores to minimize inclusion of non-porous volume. A global threshold was applied to segment PEEK from pore space and kept consistent throughout all evaluations. Pore layer morphometrics were evaluated using direct distance transformation methods [24]. Briefly, strut spacing was calculated using a maximal spheres method adapted from a trabecular spacing index. Porosity was determined by 1–BV/TV, where BV represented polymer volume and TV represented the total volume of the porous layer. Average pore layer thickness was determined using a trabecular thickness index algorithm on the filled TV of each porous layer. Pore layer interconnectivity was determined by inverting segmented pore and solid spaces and dividing the largest connected pore space volume by the total pore volume [25]. Scanning electron microscopy (SEM, Hitachi S-3700N VP-SEM) was utilized to observe the surface topography of PEEK-SP samples. Pore size was measured from SEM images as the length of the pore diagonal (n=50).

To detect changes in molecular weight due to PEEK-SP processing, gel permeation chromatography (GPC) was performed by Solvay Advanced Polymers on 100 mg samples of the isolated surface porous layer, solid core from a surface porous sample, and injection molded PEEK.

2.3 Monotonic and Fatigue Tensile Testing

Tensile tests were performed according to ASTM D638 at room temperature using a MTS Satec 20 kip (89 kN) servo-controlled, hydraulically-actuated test frame (n=5 PEEK-SP, n=5 PEEK, n=4 PMMA). The crosshead speed was 50 mm/min. Force-displacement data was used to calculate ultimate stress, elongation at break, and elastic modulus as well as generate the stress-strain curves.

Fatigue tests were run at increasingly lower stresses below the ultimate stress of the samples to generate S-N curves and determine the endurance limits of the respective samples. Fatigue tests were run on the same Satec test frame in axial stress control at a frequency of 1 Hz with a sinusoidal load. Tests were run until failure or runout. Runout was defined as greater than 1,000,000 cycles unless noted otherwise.

For monotonic and fatigue results, two representations of stress for PEEK-SP were calculated: the first using load-bearing area, A_{LB}, and the second using total area, A_T (Fig. 1). Load-bearing area was taken as the cross sectional area of the as-received dog bone before porous processing. Total area was taken as the cross sectional area of the dog bone after porous processing. Use of total area produces stress values that assume void area contributes to load-bearing, and results will consequently depend on pore layer thickness and volume fraction of porosity. Conversely, load-bearing area includes only the cross-sectional area of polymer material, including solid polymer and porous strut regions, ignoring void area in the porous layer.

2.4 Aligned Interfacial Shear

Interfacial shear testing was adapted from ASTM F1044-05 using 3M™ Scotch-weld™ 2214 Non-Metallic Filled as adhesive and a 30 kN load cell (Instron). A thin layer of adhesive was applied evenly to the surfaces of shear samples and like faces were pressed together, clamped, and placed in a vacuum oven to cure at 121°C for 1 hour. The shear test fixtures were clamped in Instron jaws and adjusted to enable horizontal alignment of the shear sample. The plane of the adhesive was coincident with the axis of loading. Cured samples were placed into custom fixtures ensuring a tight clearance fit. The fixtures were pulled apart at 2.54 mm/min until the interfacial surfaces of the samples were completely sheared. The shear stress was calculated based on the measured failure load and cross-sectional area. Shear test groups included smooth PEEK (n=4), PEEK-SP (n=8) and PEEK-BP (n=5).

2.5 Preliminary *in vivo* Animal Study

2.5.1 Surgery—An established rat femoral segmental defect model was utilized to preliminarily assess the osseointegration potential of PEEK-SP compared to smooth PEEK surfaces [26]. This model was chosen based on its previous use in characterizing bone ingrowth in porous polymeric and metallic implants [27–30]. All surgical procedures were approved by the Institutional Animal Care and Use Committee at the Georgia Institute of Technology (IACUC protocol #A11028). Briefly, bilateral 8 mm femoral defects were made in the central diaphyses of three 13-week old female Sasco Sprague-Dawley rats (Charles River), totaling six defects. Femurs were stabilized prior to defect creation using a modular plating system consisting of a polysulfone plate and two stainless steel risers. PEEK implants with one surface porous and one smooth end face were press-fit into each defect before incision closure (n=6). The orientations of surface porous faces were alternated between contralateral limbs. After surgery animals were allowed to recover and ambulate freely. Animals were injected with slow release buprenorphine at the time of surgery to relieve any pain. One animal was euthanized at 6 weeks and the remaining two were euthanized at 12 weeks.

2.5.2 *Ex vivo* µCT Imaging—Following euthanization, µCT scans were performed to assess bone ingrowth into each face of the implant. Femurs were scanned at 55 kVp and 145 µA with a 15 µm voxel size (Viva-CT, Scanco Medical). Three-dimensional reconstructions were created from two-dimensional slices thresholded to include mineral densities >50% of native cortical bone.

2.5.3 Histology—Femoral explants were fixed in formalin and stored in 70% ethanol until processing. Samples were processed through ascending grades of ethanol followed by xylene before embedding in methyl methacrylate. After embedding, rough sections were cut (Isomet® 1000 Precision Saw, Buehler) and then ground to 30 µm (EXAKT 400 CS). Sections were stained using a Goldner’s Trichrome protocol to distinguish osteoid (red) from mineralized bone (green).

2.6 Statistical Analysis

Comparisons between the strength and modulus of PEEK-SP and solid PEEK were performed with a Student's t-test. The results of the interfacial shear test were analyzed using a one-way ANOVA and Tukey post-hoc analysis (95% confidence interval). All data is expressed as average±standard deviation.

3. Results

3.1 Pore Layer Characterization

Pore morphology reliably correlated to sodium chloride crystal size (200–312 μm) and cubic nature with a pore size of 280±32 μm (Fig. 2). The pore layer was 67.3±3.1% porous and highly interconnected (99.9±0.1%) with an average strut spacing of 186.8±55.5 μm as determined by μCT. Interconnectivity values are potentially skewed slightly higher than actual values due to spatial resolution imaging limitations that may have prevented detection of thin walls between pores. However, pore interconnectivity was expected to be high due to water's high degree of pore accessibility during leaching, as evidenced by the absence of residual sodium chloride on μCT. The average thickness of the pore layer was 399.6±63.3 μm.

Table 1 shows the molecular weight of the polymer from the surface porous region, a solid region from a surface porous sample, and injection molded PEEK. The results demonstrate that the surface porous processing does not change the molecular weight of the samples.

3.2 Tensile Monotonic Testing

The creation of a surface porosity did not significantly decrease the strength of samples compared to injection molded controls when using A_{LB} (p=0.52). The ultimate tensile strength (σ_{UTS}) and elastic modulus of PEEK-SP samples were 96.11±2.61MPa and 3.36±0.30GPa compared to 97.7±1.0MPa and 3.34±0.14GPa for unprocessed solid PEEK controls, respectively, using A_{LB} (Fig. 3). However, failure strains were decreased from 20.24±2.43 to 7.79±2.25. When the total area was used in stress calculations, PEEK-SP retained 73.9% of the strength and 73.4% of the elastic modulus of solid PEEK, corresponding to a tensile strength of 71.06±2.17MPa and modulus of 2.45±0.31GPa for a porous layer that comprises approximately 20% of the sample cross sectional area.

3.3 Tensile Fatigue Testing

PEEK-SP samples demonstrated high fatigue resistance regardless of which area was used in stress calculations (σ_N = 60.0 MPa for A_{LB} and σ_N = 45.3 MPa for A_T) (Fig. 4). Further, the fatigue strength of PEEK-SP (A_{LB}) was 73% of the σ_{UTS} of smooth, injection-molded PEEK. Both PEEK and PEEK-SP experienced higher fatigue strength at similar cycle number than PMMA.

3.4 Aligned Interfacial Shear

The average shear strength of smooth PEEK, PEEK-SP, and PEEK-BP was 7.52±3.64, 23.96±2.26, and 6.81±0.81 MPa, respectively (Fig. 5). Different shear failure modes were apparent for each group. Smooth PEEK failed at the glue layer interface, PEEK-SP failed

within the porous network and within the solid region on the edges of some samples, and PEEK-BP failed in the empty bulk porous region behind the glue layer.

3.5 Implant Osseointegration

Three-dimensional μCT reconstructions of PEEK explants at 6 and 12 weeks suggested bone formation within the PEEK-SP network (Fig. 6). Bone ingrowth possessed cubic morphology similar to that of the pores, suggesting most available pore space was occupied by newly-formed bone. Cubic bone ingrowth regions were apparent at 4/6 porous interfaces and 0/6 smooth interfaces. Bone growth through the central cannula and along the outer surface of implants was present in 5/6 samples and originated from both proximal and distal ends (data not shown). Quantitative evaluation of bone ingrowth was prevented due to thresholding difficulties between PEEK and surrounding soft tissue.

Histological evidence confirmed that the mineral seen within pores on μCT reconstructions was cellularized bone (Fig. 7). At both six and twelve weeks, substantial bone formation was evident within the pore layer, with bone formation seeming to increase between the two time points. Ingrown bone was closely apposed to the pore walls and exhibited a substantial reduction in fibrous tissue formation compared to the smooth PEEK faces.

Qualitative agreement between μCT and histology was also confirmed by comparing bone ingrowth morphology at approximately the same cross sections using each technique. Mineral attenuation maps from μCT represented histological findings well and provided further validation for using μCT to detect bone ingrowth into the PEEK-SP pore layer (Fig. 7).

4. Discussion

This study sought to create a surface porosity on PEEK to promote osseointegration while maintaining the structural integrity necessary for high load-bearing orthopaedic implants. The advantages of a surface porous polymeric implant have been previously discussed in the literature [19, 31, 32]. However, no surface porous PEEK structure has been shown to provide an adequate pore network for bone ingrowth while preserving the high strength of PEEK.

Characterization of our PEEK-SP surface layer revealed pore size, porosity and interconnectivity values that have been reported to allow for cell migration, nutrient transport, and vascularization that contribute to successful bone-implant integration [19, 33]. We also show that PEEK-SP preserved a high degree of PEEK's mechanical properties, retaining over 70% of the strength and modulus of solid PEEK when total cross-sectional area A_T is used in the stress calculation. Comparatively, typical bulk porous (BP) polymers reported in the literature retain only 15–36% strength and 11–39% modulus of the unprocessed polymer, depending on porous volume fraction (Fig. 8) [3, 20, 33–38].

Although the measured strength of PEEK-SP is decreased when using the total cross-sectional area A_T, the creation of a surface porosity does not significantly decrease the strength when calculated with the load-bearing area A_{LB} (Fig. 3). The results indicate that

the stress concentration effect of pores does not negatively impact material strength. The results also indicate that PEEK-SP retains its specific strength (strength/density), meaning the introduction of porosity using this processing method only spreads the material out rather than inherently weakening it. In addition, PEEK-SP possesses mechanical properties within the range of trabecular and cortical bone (Fig. 8), a characteristic that has been suggested to improve *in vivo* functionality [33]. Mechanical properties can be tuned further by adjusting implant design parameters, such as decreasing layer thickness

Given the decrease in ductility in PEEK-SP and the inherent cyclic loading experienced by orthopaedic implants, it was important to evaluate the effect of the processing on the fatigue properties of PEEK. As shown in Fig. 4, the inherent fatigue resistance of solid PEEK was highly maintained after creation of a porous surface layer. The data also demonstrate that the fatigue resistance of PEEK-SP outperformed other clinically used orthopaedic biomaterials. PMMA, a polymer used as bone cement, did not trend towards an endurance limit and possessed much lower fatigue strength than PEEK-SP in the high cycle regime. Similarly, porous tantalum, a bulk porous metallic implant material used clinically to facilitate osseointegration, has fatigue performance almost 43% lower than surface porous PEEK at similar cycle number [39].

Because large shear stresses are experienced near bone-implant interfaces *in vivo* that can lead to micro-motion and implant loosening [40], it was essential to probe the inherent interfacial shear strength of the porous surface layer. The significant increase in interfacial shear strength of PEEK-SP compared with solid (smooth) PEEK suggests that PEEK-SP will possess the advantage of a mechanical interlock and higher bonding strength between the implant biomaterial and the surrounding natural bone once ingrowth occurs, providing greater mechanical stability at this critical interface [41]. Furthermore, PEEK-SP provides this advantage over many current techniques explored in the literature. Physical surface treatments such as plasma modification have shown increased bioactivity of PEEK implants but may not provide sufficient space for bony ingrowth and implant-bone fixation [11, 14]. In addition, PEEK implant coatings such as titanium and hydroxyapatite have demonstrated improved cellular response, [13, 42] but can be subject to delamination and decreased fatigue life [43]. Finally, sulfonation has been used to chemically modify the surface of PEEK and introduce a nanoporous surface network to improve osseointegration [32]. However, with single-micron pores that are well below the typical range for bone formation, sulfonated surface porous PEEK may not allow for the bony ingrowth that contributes to a strong mechanical interlock between the implant and bone.

The process of creating a surface porosity on PEEK implants introduces a random, topographically varied surface that may contribute to enhanced osseointegration. Such a disordered topography has been shown to improve the osteogenic response at nano- to micron-size scales [44–47]. At a larger scale, porosity has also shown increased osteogenesis compared to solid or topographically smooth surfaces [33]. Together, the literature suggests that the random, topographically varied PEEK-SP surface may enhance the cellular response, leading to more stable fixation than PEEK that is smoother at the cellular level.

Though PEEK-SP and PEEK-BP both offer the potential for bone ingrowth into the porous network, the significantly lower shear strength of PEEK-BP may limit its clinical use in rigorous loading environments. The three-fold higher shear strength of PEEK-SP could be attributed to the porous surface layer being extruded from the bulk material instead of being created with the additive or sintering techniques currently used to create PEEK-BP. Extrusion of PEEK-SP from the bulk material seamlessly integrates solid and porous regions at the molecular level and maintains the high molecular weight necessary for high strength (Table 1). Notably, the surface porous layer has higher interfacial shear strength than trabecular bone [48] (Fig. 5), which implies that failure will originate from bone itself and not the solid-porous interface even when high quality bone has fully integrated.

Preliminary *in vivo* results provide further evidence of PEEK-SP's capacity to promote bony ingrowth needed for strong implant fixation (Fig. 6, 7). Substantial bone formation within the pore layer was confirmed via μCT and histology at six and twelve weeks post-surgery. These initial *in vivo* results compare favorably with previously reported porous networks with similar architectures to PEEK-SP. For example, a porous PEEK-HA composite has been shown to facilitate bone ingrowth with close apposition to the pore walls, similar to PEEK-SP [49]. However, even the nonporous form of current PEEK-HA composites can lack the strength, ductility and fatigue resistance of PEEK-SP.

A direct comparison of PEEK-SP to porous titanium can be found in a study that used a nearly identical segmental defect model in the rat [27]. This study reports a time course of bone ingrowth close to that of PEEK-SP and also describes similar histological findings. Both studies found substantial bone formation in the central cannula and around the outside of the implants, illustrating an attempt by bone to bridge the defect. Both studies also found close bone apposition to the pore walls (or struts) with the presence of some fibrous tissue in regions where bone was absent.

Though some fibrous tissue formation was apparent within the PEEK-SP pore network, the degree to which it formed was reduced compared to the characteristic fibrous encapsulation of smooth PEEK seen in Fig. 7 and in previous studies [50, 51]. Many regions of PEEK-SP possessed pores that were completely filled with cellularized bone and no fibrous layer was observed between the bone and implant. Such reduced fibrous encapsulation combined with potentially faster bone ingrowth could increase implant stability and limit micromotion that can lead to increased inflammation and eventual implant loosening and failure [45, 52, 53].

The clinical potential of PEEK-SP is further illustrated with the clearance of this technology on a suture anchor implant through the Food and Drug Administration (FDA) in the United States (marketed as Scoria™). Despite these promising preliminary findings, further work is necessary to fundamentally understand what causes bone formation within the PEEK-SP pore layer and the quantitative mechanics behind the osseointegration of PEEK-SP [54].

5. Conclusion

We have investigated a process for selectively introducing surface porosity on PEEK that retains a substantial fraction of the solid polymer's mechanical properties. This method

provides many advantages over sintered bulk porous polymers that rely on superficial bonding between polymer particles, which severely compromises mechanical properties. The creation of a surface porosity produced samples with high tensile strength, fatigue resistance and interfacial shear strength while simultaneously providing available porosity for bone ingrowth. Preliminary *in vivo* results provided evidence of bone ingrowth into the pore network, which could lead to enhanced implant stabilization. Though the cubic morphology of ingrown bone produced by this technique provides convincing preliminary evidence of improved osseointegration, the functionality of bone ingrowth remains to be determined in future studies.

Acknowledgements

This work was supported by Solvay Advanced Polymers. The authors would like to thank K. Poynter and H. Harris for their assistance in the mechanical characterization and Laura Gartner for her assistance regarding SEM imaging. N.T.E., D.C.W., D.L.S., and K.G. are inventors of the technology disclosed in this manuscript. The technology disclosed in this manuscript has been licensed from Georgia Tech Research Corporation. N.T.E is supported by the National Science Foundation Graduate Research Fellowship under Grant No. 2013162284. F.B.T. is supported by the TI:GER program at Georgia Institute of Technology.

References

1. Place ES, Evans ND, Stevens MM. Complexity in biomaterials for tissue engineering. Nat Mater. 2009; 8:457–470. [PubMed: 19458646]
2. Nagels J, Stokdijk M, Rozing PM. Stress shielding and bone resorption in shoulder arthroplasty. Journal of Shoulder and Elbow Surgery. 2003; 12:35–39. [PubMed: 12610484]
3. Converse GL, Conrad TL, Roeder RK. Mechanical properties of hydroxyapatite whisker reinforced polyetherketoneketone composite scaffolds. Journal of the Mechanical Behavior of Biomedical Materials. 2009; 2:627–635. [PubMed: 19716108]
4. DiRienzo AL, Yakacki CM, Frensemeier M, Schneider AS, Safranski DL, Hoyt AJ, et al. Porous poly(para-phenylene) scaffolds for load-bearing orthopedic applications. Journal of the Mechanical Behavior of Biomedical Materials. 2014; 30:347–357. [PubMed: 24374261]
5. Pereira HD, Correlo V, Silva-Correia J, Oliveira J, Reis Ceng R, Espregueira-Mendes J. Migration of “bioabsorbable” screws in ACL repair. How much do we know? A systematic review. Knee Surgery, Sports Traumatology, Arthroscopy. 2013:1–9.
6. Kurtz SM, Devine JN. PEEK biomaterials in trauma, orthopedic, and spinal implants. Biomaterials. 2007; 28:4845–4869. [PubMed: 17686513]
7. Kurtz, SM. PEEK Biomaterials Handbook. William Andrew; 2011. An Overview of PEEK Biomaterials; p. 1-8.
8. Williams DF, McNamara A, Turner RM. Potential of polyetheretherketone (PEEK) and carbon-fibrereinforced PEEK in medical applications. Journal of Materials Science Letters. 1987; 6:188–190.
9. Arima Y, Iwata H. Effect of wettability and surface functional groups on protein adsorption and cell adhesion using well-defined mixed self-assembled monolayers. Biomaterials. 2007; 28:3074–3082. [PubMed: 17428532]
10. Ha SW, Hauert R, Ernst KH, Wintermantel E. Surface analysis of chemically-etched and plasma-treated polyetheretherketone (PEEK) for biomedical applications. Surface & Coatings Technology. 1997; 96:293–299.
11. Briem D, Strametz S, Schroder K, Meenen NM, Lehmann W, Linhart W, et al. Response of primary fibroblasts and osteoblasts to plasma treated polyetheretherketone (PEEK) surfaces. Journal of Materials Science-Materials in Medicine. 2005; 16:671–677. [PubMed: 15965600]
12. Poulsson AHC, Eglin D, Zeiter S, Camenisch K, Sprecher C, Agarwal Y, et al. Osseointegration of machined, injection moulded and oxygen plasma modified PEEK implants in a sheep model. Biomaterials. 2014; 35:3717–3728. [PubMed: 24485795]

13. Han C-M, Lee E-J, Kim H-E, Koh Y-H, Kim KN, Ha Y, et al. The electron beam deposition of titanium on polyetheretherketone (PEEK) and the resulting enhanced biological properties. Elsevier. 2009; 31:3465–3470.
14. Ha SW, Kirch M, Birchler F, Eckert KL, Mayer J, Wintermantel E, et al. Surface activation of polyetheretherketone (PEEK) and formation of calcium phosphate coatings by precipitation. Journal of Materials Science-Materials in Medicine. 1997; 8:683–690. [PubMed: 15348819]
15. Bakar A, Cheng M, Tang S, Yu S, Liao K, Tan C, et al. Tensile properties, tension–tension fatigue and biological response of polyetheretherketone–hydroxyapatite composites for load-bearing orthopedic implants. Biomaterials. 2003; 24:2245–2250. [PubMed: 12699660]
16. Shenton MJ, Stevens GC. Surface modification of polymer surfaces: atmospheric plasma versus vacuum plasma treatments. Journal of Physics D: Applied Physics. 2001; 34:2761.
17. Poulsson, AHC.; Richards, RG. PEEK Biomaterials Handbook. William Andrew; 2011. Surface Modifications Techniques of Polyaryletheretherketone, Including Plasma Surface Treatment; p. 145-162.
18. Karageorgiou V, Kaplan D. Porosity of 3D biomaterial scaffolds and osteogenesis. Biomaterials. 2005; 26:5474–5491. [PubMed: 15860204]
19. Jarman-Smith, Marcus; Brady, Mark; Kurtz, Steven M.; Cordara, NM.; Walsh, WR. Porosity in Polyaryletheretherketone. In: Kurtz, SM., editor. PEEK Biomaterials Handbook. Elsevier Science; 2011. p. 181-200.
20. Landy BC, Vangordon SB, McFetridge PS, Sikavitsas VI, Jarman-Smith M. Mechanical and in vitro investigation of a porous PEEK foam for medical device implants. Journal of applied biomaterials & functional materials. 2013; 11:e35–e44. [PubMed: 23413130]
21. Sinclair SK, Konz GJ, Dawson JM, Epperson RT, Bloebaum RD. Host bone response to polyetheretherketone versus porous tantalum implants for cervical spinal fusion in a goat model. Spine. 2012; 37:E571–E580. [PubMed: 22146277]
22. Zhou J, Lin H, Fang T, Li X, Dai W, Uemura T, et al. The repair of large segmental bone defects in the rabbit with vascularized tissue engineered bone. Biomaterials. 2010; 31:1171–1179. [PubMed: 19880177]
23. Muller U, Imwinkelried T, Horst M, Sievers M, Graf-Hausner U. Do human osteoblasts grow into open-porous titanium? European cells & materials. 2006; 11:8–15. [PubMed: 16425146]
24. Hildebrand T, Laib A, Muller R, Dequeker J, Ruegsegger P. Direct three-dimensional morphometric analysis of human cancellous bone: microstructural data from spine, femur, iliac crest, and calcaneus. Journal of bone and mineral research : the official journal of the American Society for Bone and Mineral Research. 1999; 14:1167–1174.
25. Lin AS, Barrows TH, Cartmell SH, Guldberg RE. Microarchitectural and mechanical characterization of oriented porous polymer scaffolds. Biomaterials. 2003; 24:481–489. [PubMed: 12423603]
26. Oest ME, Dupont KM, Kong HJ, Mooney DJ, Guldberg RE. Quantitative assessment of scaffold and growth factor-mediated repair of critically sized bone defects. Journal of orthopaedic research : official publication of the Orthopaedic Research Society. 2007; 25:941–950. [PubMed: 17415756]
27. Van der Stok J, Van der Jagt OP, Amin Yavari S, De Haas MF, Waarsing JH, Jahr H, et al. Selective laser melting-produced porous titanium scaffolds regenerate bone in critical size cortical bone defects. Journal of orthopaedic research : official publication of the Orthopaedic Research Society. 2013; 31:792–799. [PubMed: 23255164]
28. Dupont KM, Sharma K, Stevens HY, Boerckel JD, García AJ, Guldberg RE. Human stem cell delivery for treatment of large segmental bone defects. Proceedings of the National Academy of Sciences. 2010; 107:3305–3310.
29. Rai B, Oest ME, Dupont KM, Ho KH, Teoh SH, Guldberg RE. Combination of platelet-rich plasma with polycaprolactone-tricalcium phosphate scaffolds for segmental bone defect repair. Journal of biomedical materials research Part A. 2007; 81:888–899. [PubMed: 17236215]
30. Wojtowicz AM, Shekaran A, Oest ME, Dupont KM, Templeman KL, Hutmacher DW, et al. Coating of biomaterial scaffolds with the collagen-mimetic peptide GFOGER for bone defect repair. Biomaterials. 2010; 31:2574–2582. [PubMed: 20056517]

31. He Q, Chen HL, Huang L, Dong JJ, Guo DG, Mao MM, et al. Porous Surface Modified Bioactive Bone Cement for Enhanced Bone Bonding. PLoS One. 2012; 7
32. Zhao Y, Wong HM, Wang WH, Li PH, Xu ZS, Chong EYW, et al. Cytocompatibility, osseointegration, and bioactivity of three-dimensional porous and nanostructured network on polyetheretherketone. Biomaterials. 2013; 34:9264–9277. [PubMed: 24041423]
33. Karageorgiou V, Kaplan D. Porosity of 3D biomaterial scaffolds and osteogenesis. Biomaterials. 2005; 26:5474–5491. [PubMed: 15860204]
34. Shimko DA, Shimko VF, Sander EA, Dickson KF, Nauman EA. Effect of porosity on the fluid flow characteristics and mechanical properties of tantalum scaffolds. Journal of Biomedical Materials Research Part B: Applied Biomaterials. 2005; 73B:315–324.
35. Eshraghi S, Das S. Mechanical and microstructural properties of polycaprolactone scaffolds with one-dimensional, two-dimensional, and three-dimensional orthogonally oriented porous architectures produced by selective laser sintering. Acta biomaterialia. 2010; 6:2467–2476. [PubMed: 20144914]
36. Kurtz, SM. UHMWPE Biomaterials Handbook: Ultra High Molecular Weight Polyethylene in Total Joint Replacement and Medical Devices. Elsevier Science; 2009. A Primer on UHMWPE; p. 1-6.
37. Wang L, Yoon DM, Spicer PP, Henslee AM, Scott DW, Wong ME, et al. Characterization of porous polymethylmethacrylate space maintainers for craniofacial reconstruction. Journal of biomedical materials research Part B, Applied biomaterials. 2013; 101:813–825.
38. Suwanprateeb J, Chumnanklang R. Three-dimensional printing of porous polyethylene structure using water-based binders. Journal of biomedical materials research Part B, Applied biomaterials. 2006; 78:138–145.
39. Zardiackas LD, Parsell DE, Dillon LD, Mitchell DW, Nunnery LA, Poggie R. Structure, metallurgy, and mechanical properties of a porous tantalum foam. Journal of Biomedical Materials Research. 2001; 58:180–187. [PubMed: 11241337]
40. Cheal EJ, Spector M, Hayes WC. Role of loads and prosthesis material properties on the mechanics of the proximal femur after total hip arthroplasty. Journal of orthopaedic research : official publication of the Orthopaedic Research Society. 1992; 10:405–422. [PubMed: 1569504]
41. Bobyn JD, Pilliar RM, Cameron HU, Weatherly GC, Kent GM. The effect of porous surface configuration on the tensile strength of fixation of implants by bone ingrowth. Clinical orthopaedics and related research. 1980:291–298. [PubMed: 7408314]
42. Yao C, Storey D, Webster TJ. Nanostructured metal coatings on polymers increase osteoblast attachment. Int J Nanomedicine. 2007; 2:487–492. [PubMed: 18019846]
43. Robotti, P.; Zappini, G. Thermal Plasma Spray Deposition of Titanium and Hydroxyapatite on Polyaryletheretherketone Implants. In: Kurtz, SM., editor. PEEK Biomaterials Handbook. William Andrew; 2011. p. 119-144.
44. Shalabi MM, Gortemaker A, Van't Hof MA, Jansen JA, Creugers NHJ. Implant surface roughness and bone healing: a systematic review. Journal of Dental Research. 2006; 85:496–500. [PubMed: 16723643]
45. Gittens RA, Olivares-Navarrete R, Schwartz Z, Boyan BD. Implant osseointegration and the role of microroughness and nanostructures: Lessons for spine implants. Acta biomaterialia. 2014
46. Dalby MJ, Gadegaard N, Tare R, Andar A, Riehle MO, Herzyk P, et al. The control of human mesenchymal cell differentiation using nanoscale symmetry and disorder. Nature Materials. 2007; 6:997–1003.
47. Meyer U, Buchter A, Wiesmann HP, Joos U, Jones DB. Basic reactions of osteoblasts on structured material surfaces. European cells & materials. 2005; 9:39–49. [PubMed: 15852237]
48. Goldstein SA. The mechanical properties of trabecular bone: dependence on anatomic location and function. Journal of biomechanics. 1987; 20:1055–1061. [PubMed: 3323197]
49. Abu Bakar MS, Cheng MHW, Tang SM, Yu SC, Liao K, Tan CT, et al. Tensile properties, tension– tension fatigue and biological response of polyetheretherketone–hydroxyapatite composites for loadbearing orthopedic implants. Biomaterials. 2003; 24:2245–2250. [PubMed: 12699660]

50. Nieminen T, Kallela I, Wuolijoki E, Kainulainen H, Hiidenheimo I, Rantala I. Amorphous and crystalline polyetheretherketone: Mechanical properties and tissue reactions during a 3-year follow-up. Journal of Biomedical Materials Research Part A. 2008; 84A:377–383. [PubMed: 17618477]

51. Jockisch KA, Brown SA, Bauer TW, Merritt K. Biological response to chopped-carbon-fiberreinforced peek. Journal of Biomedical Materials Research. 1992; 26:133–146. [PubMed: 1569111]

52. Götz HE, Müller M, Emmel A, Holzwarth U, Erben RG, Stangl R. Effect of surface finish on the osseointegration of laser-treated titanium alloy implants. Biomaterials. 2004; 25:4057–4064. [PubMed: 15046896]

53. Aspenberg P, Goodman S, Toksviglarsen S, Ryd L, Albrektsson T. INTERMITTENT MICROMOTION INHIBITS BONE INGROWTH - TITANIUM IMPLANTS IN RABBITS. Acta Orthopaedica Scandinavica. 1992; 63:141–145. [PubMed: 1590046]

54. Guldberg RE, Richards M, Caldwell NJ, Kuelske CL, Goldstein SA. Trabecular bone adaptation to variations in porous-coated implant topology. Journal of biomechanics. 1997; 30:147–153. [PubMed: 9001935]

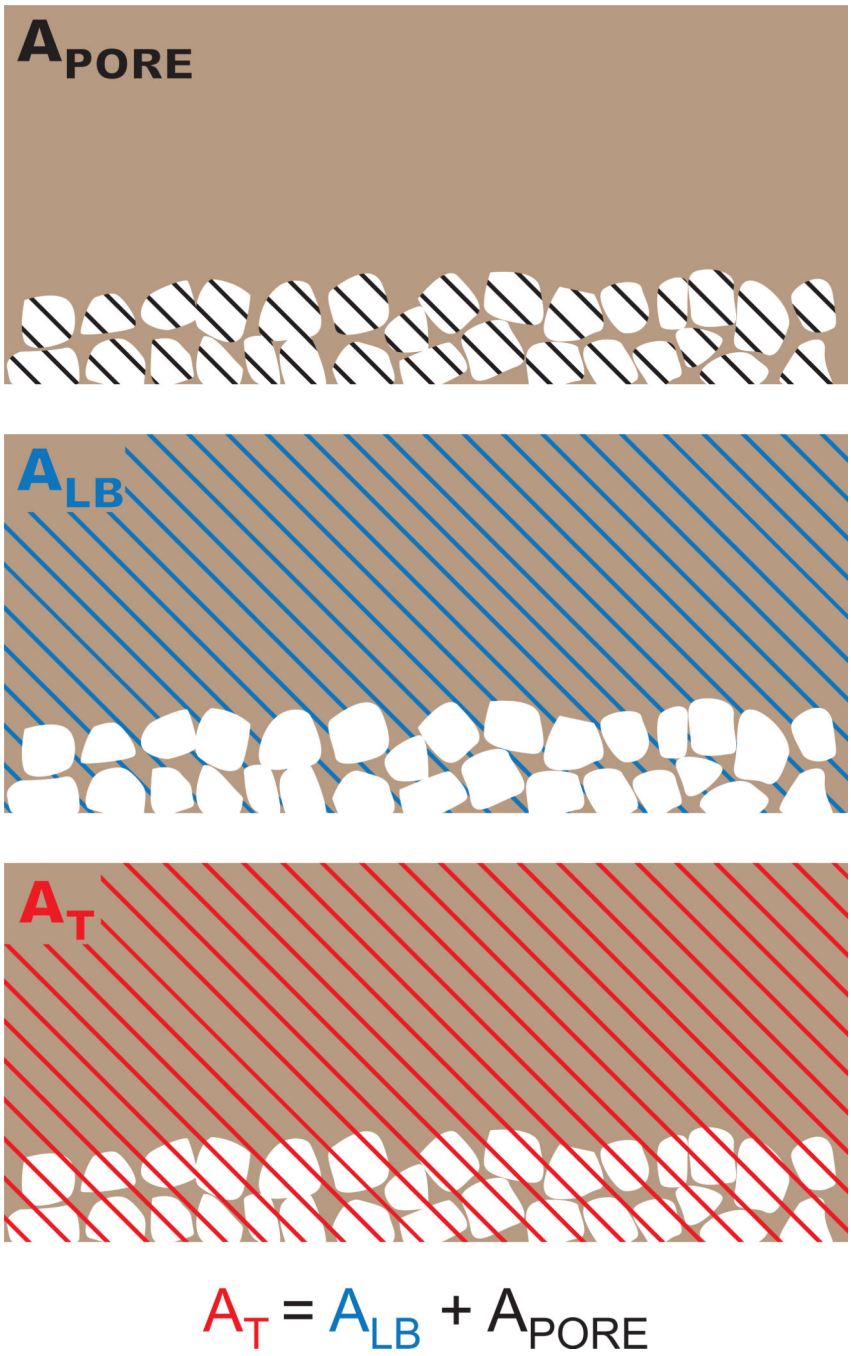

Fig. 1.

Schematic of the PEEK-SP cross-sectional areas used in stress calculations. The processing increases cross-sectional areas due to the creation of pores. However, the load-bearing area, A_{LB}, is representative of the initial area of PEEK material, assuming volume conservation. The total area, A_T, is the sum of the load-bearing area and the area of the pore network, A_{PORE}.

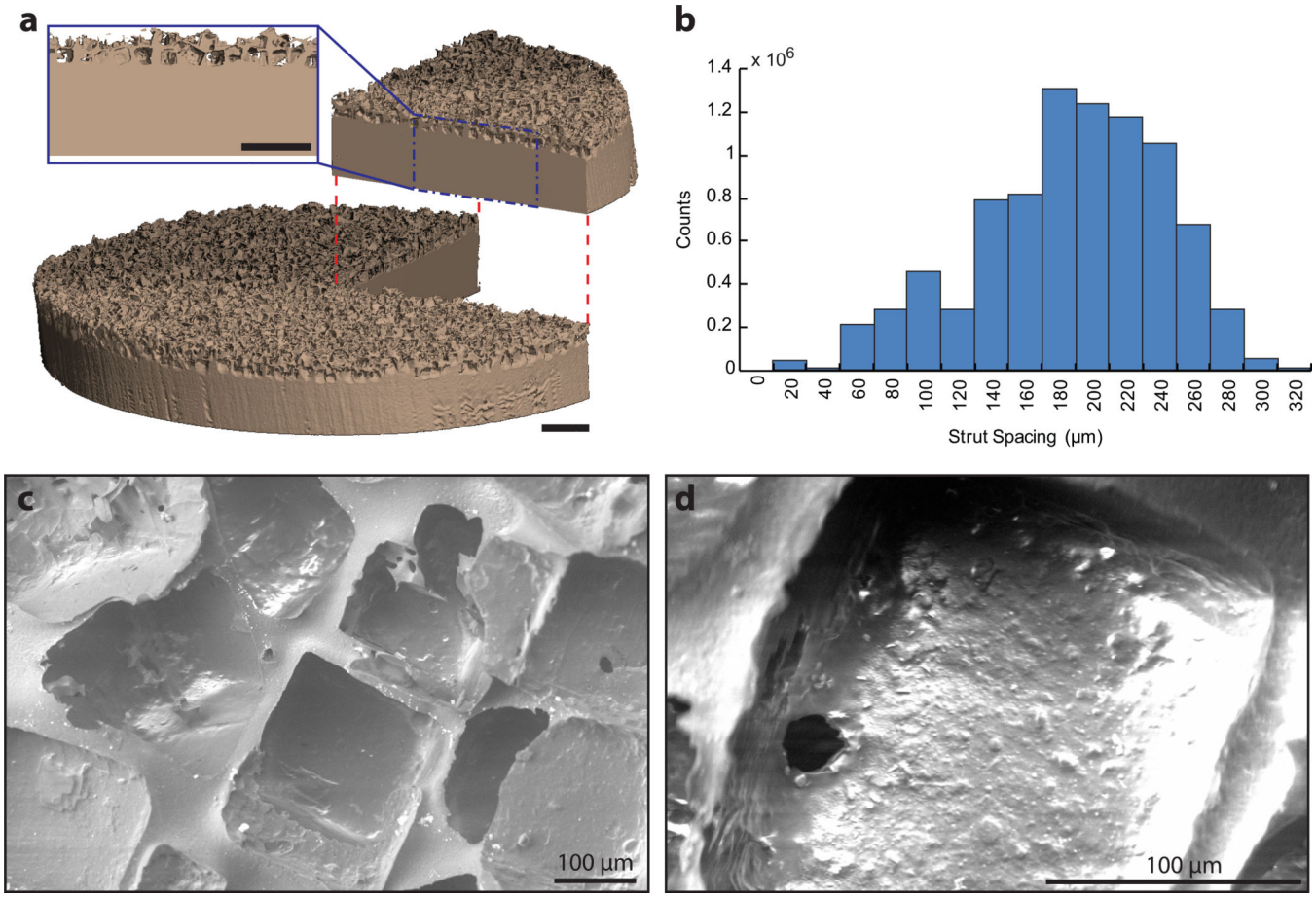

Fig. 2.

Microstructural characterization of PEEK-SP: (a) μCT reconstruction of PEEK-SP structure showing representative pore layer cross-section. Note the cubic pore morphology due to cubic sodium chloride crystals. Scale bar is 1 mm. (b) Strut spacing histogram as characterized by micro-CT. (c,d) SEM micrographs of the PEEK-SP pore network. Images confirm cubic pore morphology and pore interconnectivity detected by μCT.

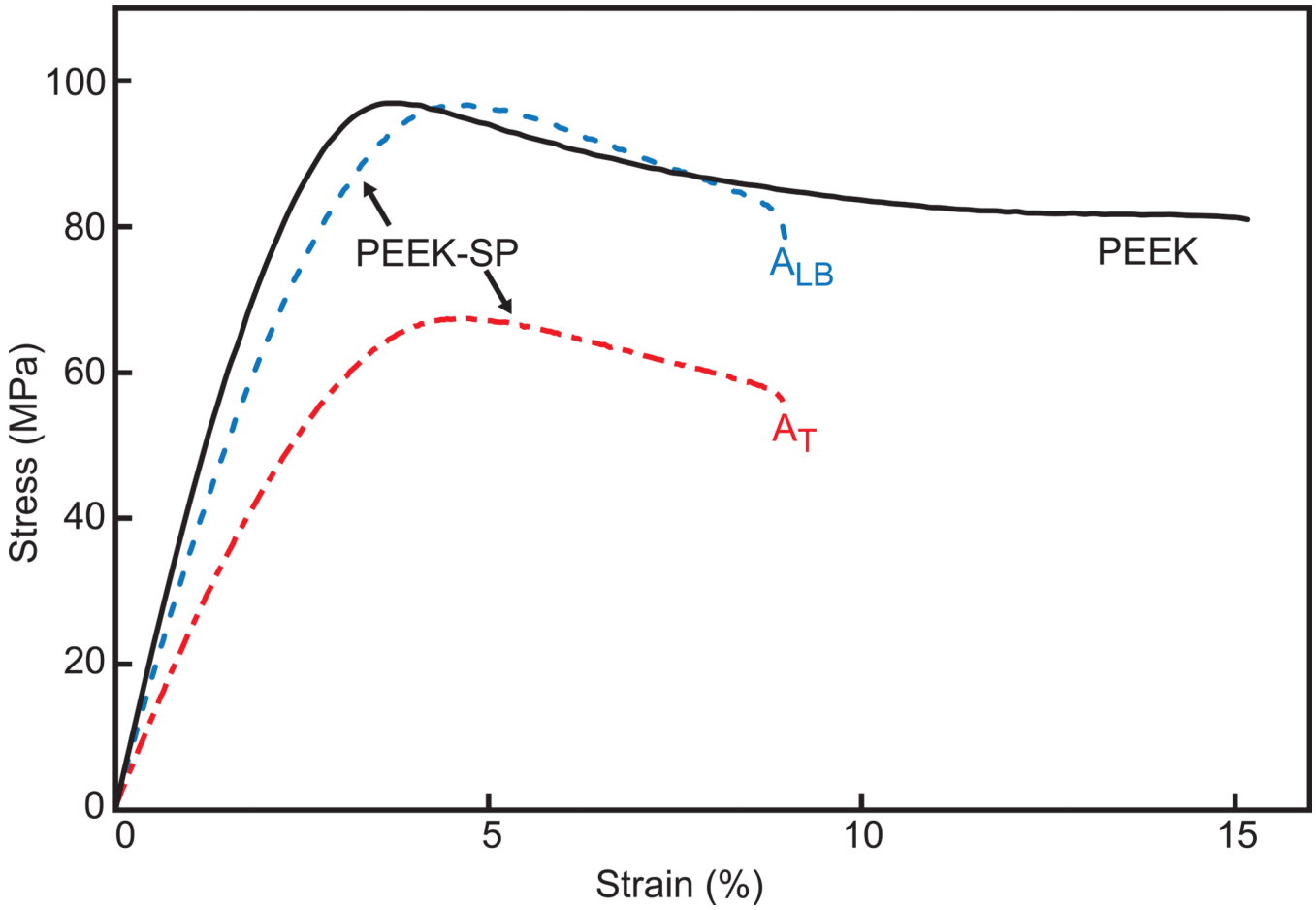

Fig. 3.
Representative stress-strain curves of solid PEEK and PEEK-SP calculated using both A_{LB} and A_T.

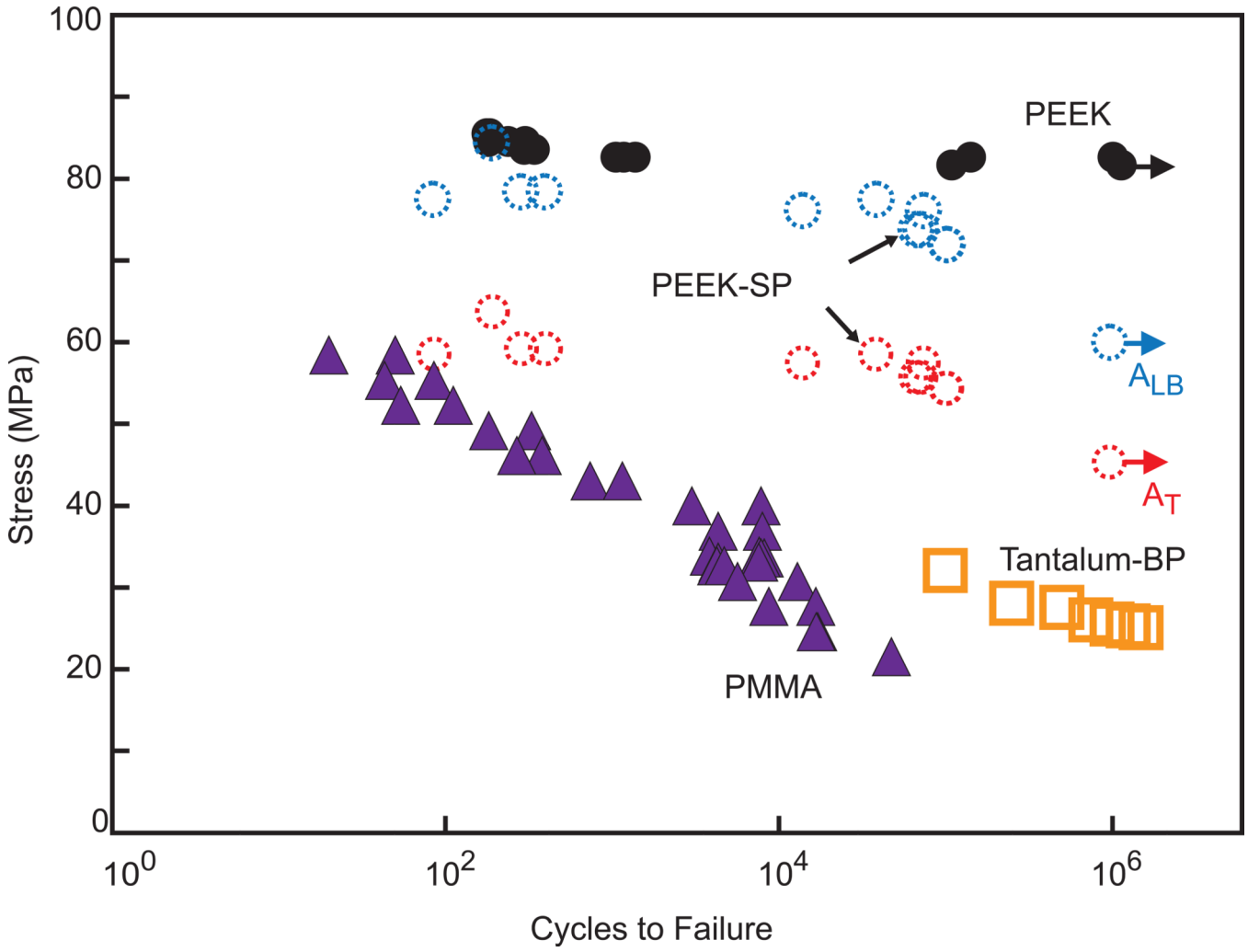

Fig. 4.

S-N curve comparing the fatigue behavior of PEEK-SP using the load-bearing, A_{LB}, and the total area, A_T, to solid PEEK, PMMA, and bulk porous tantalum tested by another group [39]. Arrows denote tests that were halted after reaching 10^6 cycles (solid PEEK, PEEK-SP), which is defined as the runout stress.

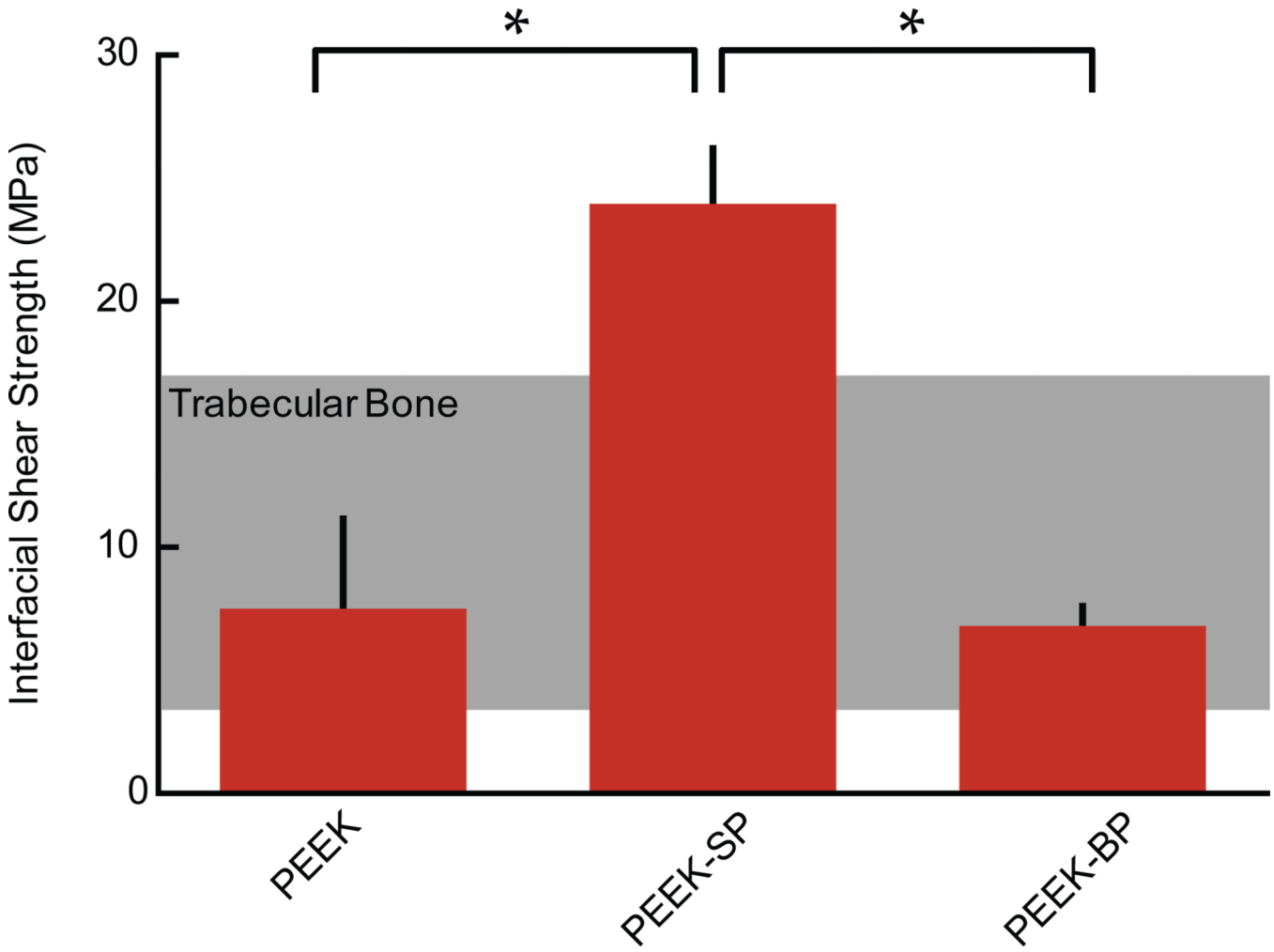

Fig. 5.

Interfacial shear strength of PEEK-SP compared to smooth PEEK and sintered PEEK-BP with the shear strength of trabecular bone shown in the shaded region [48]. Asterisks (*) indicate $p < 0.05$.

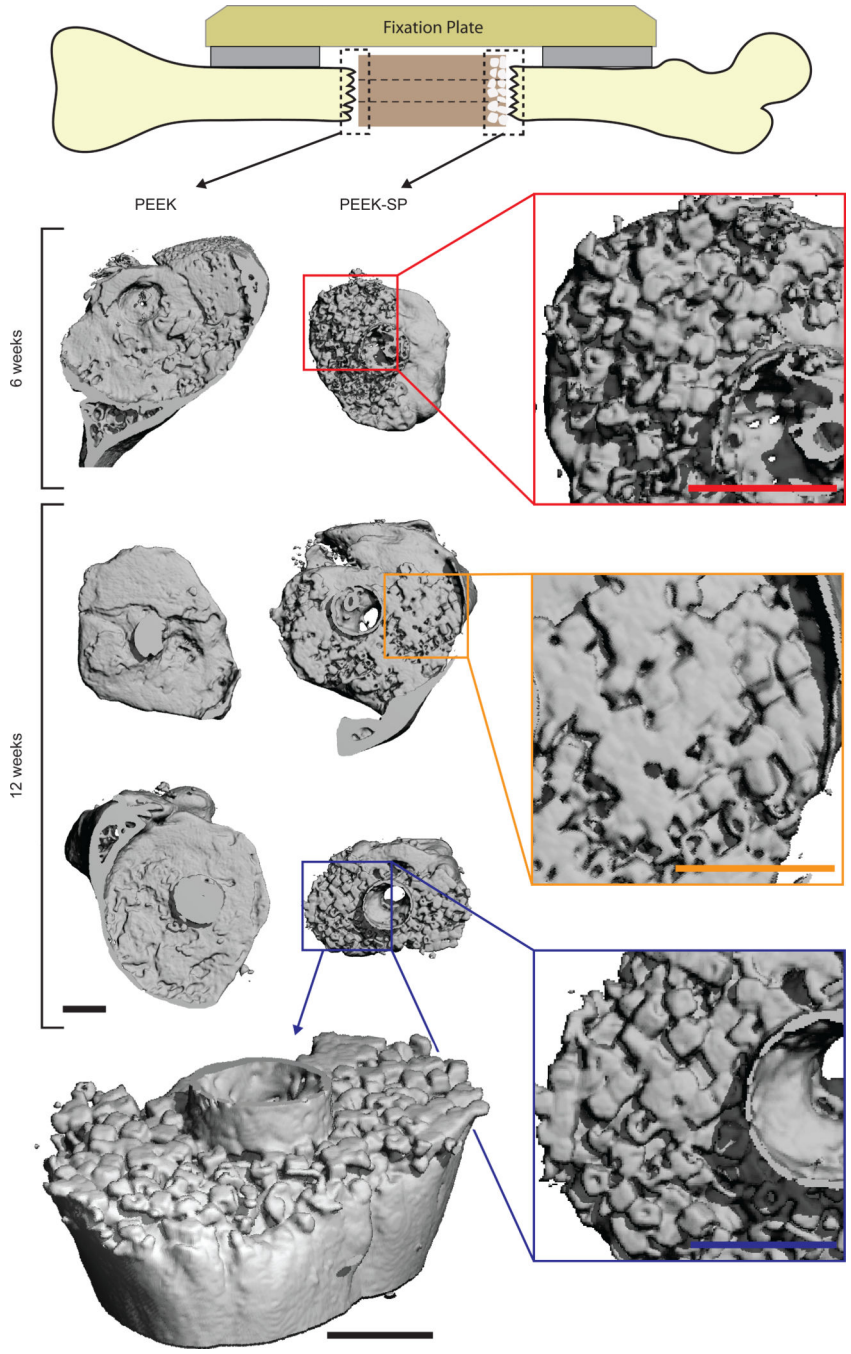

Fig. 6.

μCT reconstructions of bone growth into PEEK-SP and adjacent to smooth PEEK surfaces (dashed boxes) at 6 and 12 weeks show the extent of bone ingrowth. Images are oriented with the lateral side on top. Insets show magnified views of ingrown bone. PEEK implants are not depicted due to thresholding difficulties of μCT reconstructions. An angled view is presented to visualize the extent of bone intrusion into the porous surface layer. Note the cubic morphology of bone in the surface porous PEEK samples, suggesting complete growth into the cubic pores. Scale bars on μCT images are 1 mm.

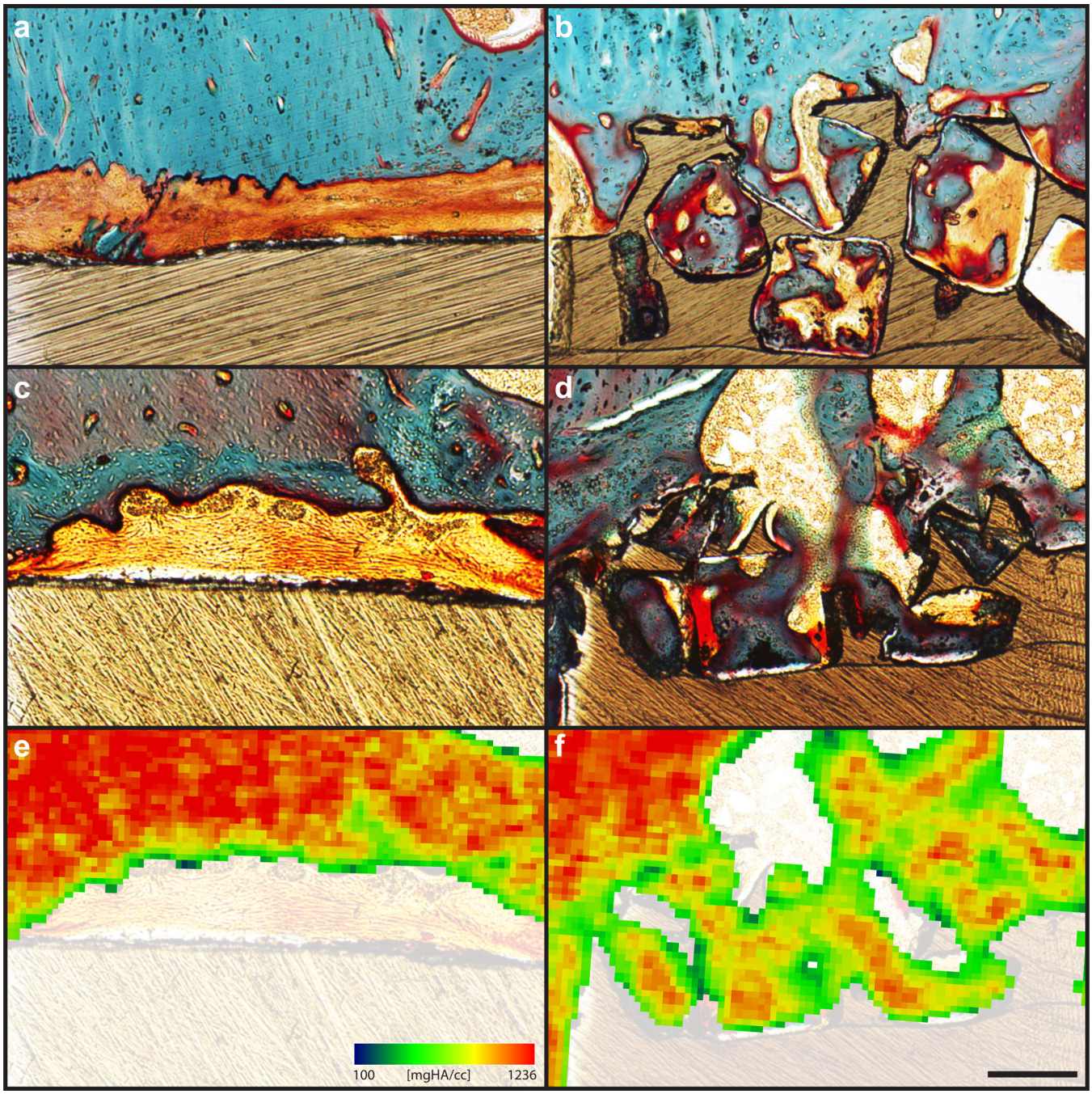

Fig. 7.

Bone ingrowth of PEEK-SP and smooth PEEK surfaces: (a,c) Representative histological images of fibrous tissue formation on smooth PEEK faces at six and twelve weeks, respectively. (b,d) Representative histological images of bone ingrowth within PEEK-SP faces at six and twelve weeks, respectively. Osteoid stained deep red; mineralized bone stained green; fibrous tissue stained light orange; and PEEK material is seen in brown. (e,f) Representative mineral attenuation maps from μCT at approximately the same cross sections

as (c,d). Blue represents lower mineral density and red indicates high mineral density. Scale bar is 200 μm.

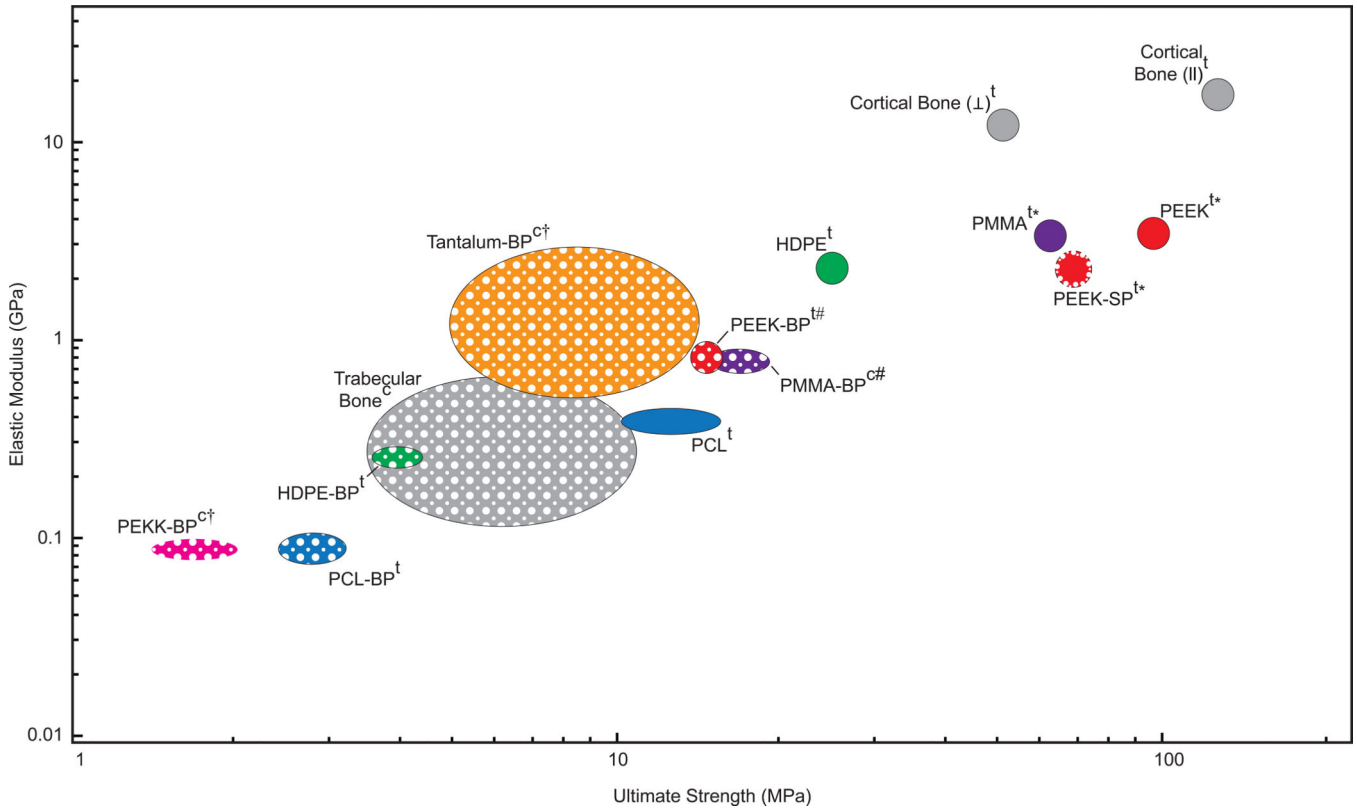

Fig. 8.

Ashby plot of elastic moduli and ultimate strengths for several orthopaedic biomaterials and bone that have been reported in the literature [3, 20, 33–38]. Solid-filled ellipses represent fully dense materials and porous-filled ellipses represent porous materials. While cortical bone does possess low porosity, it is grouped with the fully dense materials for this comparison. Each material, with the exception of porous tantalum and polyether-ketone-ketone (PEKK), has both solid and porous properties included to illustrate the reduction in properties due to porosity. PEEK-SP is indicated by a porous layer outlining the solid-filled circle. Superscript ‘t’ refers to materials tested in tension and ‘c’ indicates compression. Daggers (†) indicate yield strengths where ultimate strength was not reported. Pound signs (#) indicate bending modulus when elastic modulus was not reported. Asterisks (*) indicate values tested by our group. Ellipse central location and size represents reported mean and plus or minus one standard deviation, respectively, where available.

Table 1

Molecular weight distribution.

	M_n (g/mol)	M_w (g/mol)	PDI[d]
Porous[a]	44 753	100 032	2.24
Solid[b]	45 717	99 449	2.18
Injection Molded[c]	46 208	98 846	2.14

[a] Porous region of PEEK-SP

[b] Solid region of PEEK-SP

[c] Injection molded PEEK without surface porous treatment

[d] Polydispersity index, PDI = Mw/Mn